EUROPEAN COMMISSION

Community Research

SEVENTH FRAMEWORK PROGRAMME

ARCHER

Collaborative Project

Co-funded by the European Commission under the
Euratom Research and Training Programme on Nuclear Energy
within the Seventh Framework Programme

Grant Agreement Number: 269892
Start date: 01/02/2011 Duration: 48 Months

www.archer-project.eu

Archer
Advanced Reactor
for Cogeneration of
Heat & Electricity-R&D

BISE Test Facility Description Report

François Gensdarmes (IRSN), Audrey Roynette (IRSN), Samuel Peillon (IRSN)

ARCHER project – Contract Number: 269892
Advanced High-Temperature Reactors for Cogeneration of Heat and Electricity R&D
EC Scientific Officer: Dr. Panagiotis Manolatos

Document title	BISE test facility description report
Author(s)	François Gensdarmes (IRSN), Audrey Roynette (IRSN), Samuel Peillon (IRSN)
Number of pages	29
Document type	Deliverable
Work Package	WP 2.3.3
Document number	D23.31 – revision 0
Issued by	IRSN
Date of completion	12/03/2012
Dissemination level	Restricted to the partners of the ARCHER project/Public

Summary

This report describes the design of BISE (Blowing facility for airborne release) experimental set-up used to study the particle resuspension phenomena by airflow within the ARCHER (Advanced High-Temperature Reactors for Cogeneration of Heat and Electricity R&D) project. BISE allows producing turbulent airflows with mean velocities ranging from 0.5 $m.s^{-1}$ to 10 $m.s^{-1}$. Careful characterisations of the boundary layer and velocity fields are presented.

Approval

Rev.	Short description	First author	WP Leader	SP leader	Coordinator
0	First issue	François Gensdarmes (IRSN) 15/03/2012		Norbert Kohtz (TUV – Rheinland) 12/03/12	Sander De Groot (NRG) 12/03/12

Distribution list

Name	Organisation	Comments
P. Manolatos	EC DG RTD	
All technical participants	ARCHER	
Steering Committee members	ARCHER	

Table of contents

List of figures

1. Introduction

The resuspension of particles in the atmosphere when exposed to a gas flow is a complex phenomenon, both theoretically in terms of adhesion and detachment of particles from a surface as well as in terms of the various models developed in this field.

However, the work published by many researchers over the past few years, represents a remarkable advance in our understanding of the mechanism of particle resuspension. Indeed, whether addressing the very pragmatic and simple lifting of the particle from the surface based on a balance of forces (the quasi-static model), or a summation of the particle's energy (dynamic model), researchers have made theoretical developments by focussing on the imperceptible movements of the particle before it departs in the free stream. Thus by integrating the components of the forces in the mechanism and by combining the two basic concepts involved in re-entrainment (balance of forces and conservation of energy), resuspension models have been developed which describe the phenomenon in more detail. These more realistic models seem extremely promising. The model of Reeks and Hall (2001) combined with the adhesive force correlations established by Biasi *et al*. (2001) appears to be the most realistic model, since it has been validated by four series of experiments reported in the literature (Braaten, Hall, STORM and ORNL) for single layer and multilayered deposits of particles having diameters between 0.1 µm and 30 µm deposited onto rough surfaces.

However, although the Rock 'n Roll model from Reeks and Hall (2001) has been validated for multilayered deposits of sub-micron particles, this theoretical development has not been verified for larger particle sizes. Moreover, it was elaborated for an isolated spherical particle on a surface. Hence it does not consider the additional forces and parameters which arise when the particles are deposited in layers. Fromentin (1989), however, studied these additional characteristics in the theoretical and experimental investigation which he undertook on resuspension of particles from a multilayer deposit. Later confirmed by other authors (including Biasi *et al*., 2001), it explains why resuspension of such deposits only occurs for particles in the upper layer, i.e. the layer in direct contact with the airflow. He also highlighted the fact that the resuspended fraction KR initially increases with time but quickly becomes stable; he attributed this stabilization of the resuspension to a hardening in the distribution of adhesive forces from the lower layers. The author experimentally verified his theoretical treatment for particles with diameters between 0.4 µm and 4.3 µm; he developed a correlation of the mean flow rate for resuspension with the influence of velocity and duration of exposure, but not with the particle size.

It is important to note that the time parameter mainly enters into the Fromentin correlation through the fact that the resuspension is described by its mean flowrate. To analyse the results in the literature, it is therefore essential to homogenize all the information by expressing resuspension only in terms of the resuspended fraction.

Although the Rock 'n Roll model and the Fromentin correlation seemed promising, they have not been validated in multilayer deposits for particle sizes greater than several microns. Neither have they been verified for clusters of particles, such as piles of powder. The only studies treating these forms of more generic piles have been carried out in the field of sediments transported by the wind, but the size of particles studied there is clearly much larger (> 250 µm).

Finally, one essential point comes out of our literature study: there is a clear lack of understanding which parameters are likely to influence resuspension. Indeed, the disagreements between the various studies arise in relation to the importance attached to the various parameters influencing the phenomenon. However, none of the studies investigate their relative influence.

Many authors have carried out theoretical and experimental studies in order to appreciate the influence of parameters such as particle size, air velocity or the duration of exposure to the air flow.

As a result of our literature study, we are nevertheless able to select the following parameters for our investigation:

- parameters which demonstrate a degree of influence:
  - the velocity of the airflow,
  - the particle size,
- parameters whose influence needs to be characterized in more detail:
  - the duration of exposure (this seems to have a very targeted influence at the start of the experiment),
  - acceleration,
  - porosity of the deposit (from Friess and Yadigaroglu, 1998),
  - surface roughness (considered in several models),
- parameters which have hardly been investigated, if at all:
  - the "pile of powder" deposit configuration,
  - shape of the particles,
  - water content (directly linked to the capillary force),
  - turbulence (emphasized theoretically).

The other parameters are often the consequence of additional factors (saltation due to the size of particles or deformation of the deposit due to the time of exposure, the relative humidity the particle size or the size of the deposit). As much as possible, we will try to observe and control these.

However, as we have seen in this section, the experiments that have previously been carried out were performed under many different experimental conditions, very often preventing comparisons between them. The majority of researchers have targeted their investigations on a single parameter (the velocity in some cases, but the particle size in the majority of experiments).

Under these conditions, it is difficult to evaluate the relative effect of these parameters on the resuspension and classify them in order of importance. To date, the existing literature on resuspension by airflows suffers from a significant lack of experimental data to resolve this problem. However, in terms of the ten parameters which we have selected above, the development of resuspension models for multilayer deposits or piles of powder should be improved if we can understand the relative effects of these factors on resuspension.

This is why we propose to carry out an experimental study which can differentiate the main effects of the parameters on the resuspension of a particulate contamination by an airflow. To achieve this, we have developed an experimental apparatus suitable to our needs (Alloul-Marmor, 2002). It is described in the next section.

2. The BISE experimental facility

The general aim of the work is to study resuspension by airflow of non-radioactive polydispersed particles deposited on a surface, by studying the parameters likely to influence this phenomenon. Studying such a phenomenon in the laboratory requires a special experimental wind-tunnel type facility. Our facility, which responds to these criteria, is called BISE (**B**lowing facility for a**I**rborne relea**SE**).

2.1. Description

Figure 1 is a general diagram of the BISE facility. The facility contains an open circuit test air duct around 5 m long. Air is circulated in the test bench by suction, provided by a vacuum pump located in the downstream section of BISE.

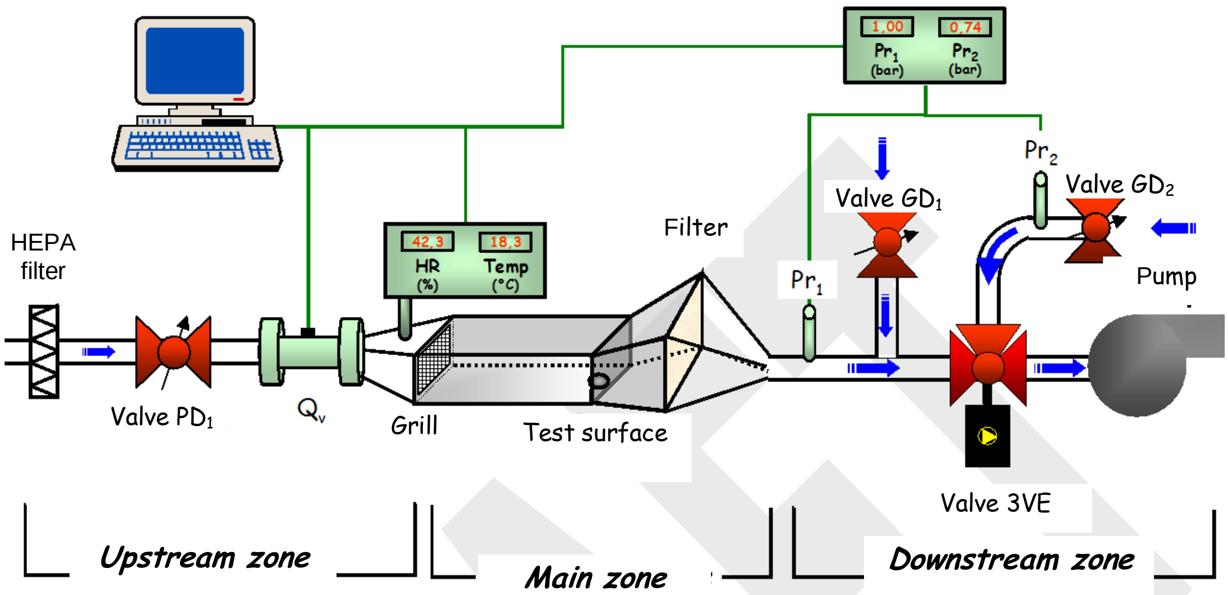

Figure 1 – Diagram of the BISE experimental facility (Blowing facility for aIrborne releaSE)

The main zone of the facility is composed of two Plexiglas parts. The first is a horizontal rectangular parallelepiped duct, 40 cm long, 12 cm wide and 7 cm high. These dimensions were mainly determined by the fact that the physical phenomenon studied takes place in the immediate proximity of the surface. Added to this, the range of air velocities to be researched (0.5 m/s to 10 m/s) requires the availability of a large flow at high velocity (of order 300 m^3/h).

Immediately before the exit plane from the straight parallelepiped section is the test surface, where the test powder will be deposited. A diagram of this zone is given in figure 2.

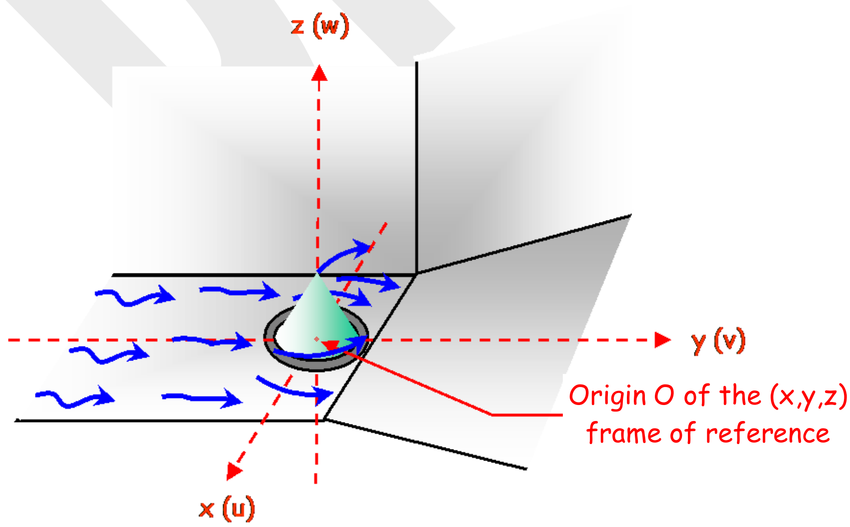

Figure 2 – Expanded view of the powder cone deposited on the test surface in BISE facility

This aluminium test surface is circular (diameter 4 cm) and movable. It provides the possibility to change the surface of the bed (aluminium, stainless steel or other material) or, uniquely, to modify its roughness parameter. The centre of this test surface is aligned on the axis of the principle direction of flow, on the lower surface of the duct. This point is taken as the geometric reference in the BISE facility.

The second part of the main zone of this apparatus is in the shape of a trapezoidal rectangular pyramid. A sampling filter, 18 cm high and 22 cm wide, is positioned vertically in the plane of the exit from this zone. The distance between the test surface and the filter carrier is 12 cm. The diverging geometry of this piece is imposed by the flow velocities planned for the experiments, the type of filters used (which requires high pressure drops) and the commercial vacuum pumps available. The technical solution envisaged (increasing of the surface area of the sampling filter) did not influence the local resuspension phenomenon. This second piece was required so that the experiments with specific analysis of the filter could be performed.

Upstream of the main zone (see figure 1, upstream zone) is a High Efficiency Particulate Air (HEPA) filter which ensures that the air in the test bench is clean, without contamination by parasite particles. A low flow regulating valve (PD_1) is followed by a turbine volumetric flowmeter (Schlumberger Fluxi 2100). This controls the volumetric flow rate, Q_v, established in BISE during the course of an experiment. The flowmeter operates by measuring the rotation frequency of its turbine. If the area of the cross-section of the test duct at the test surface location is known, then the measured flow rate allows the value of the mean velocity in this plane to be calculated.

A grid with a mesh of 1 mm squares and thickness 0.8 mm ("Stainless steel wire cloth 304" from Saulas) is located upstream of the straight section of the parallelepiped test duct. This grid is intended both to homogenize the air velocities over the cross-section of the test duct, and also to induce turbulence in the plane where the powder is positioned, which will be as uniform and isotropic as possible.

Downstream from the main zone (see figure 1, downstream zone) is a device for adjusting the overall flow. It is essential to have this device because the flow rate of the vacuum pump is not adjustable. The device consists of two identical regulating valves, one of which is positioned on the main duct (GD_1) and the other on a branch duct (GD_2). Switching between the two ducts is achieved by a 3-way electro-pneumatic valve with adjustable opening speed. This configuration was chosen for two reasons:

- To provide the same pressure drop in the two circuits for a given air velocity in the main circuit, i.e. $Pr_1 = Pr_2$. Hence, the vacuum pump is always subject to the same experimental conditions during switching of the air supply between the two circuits.
- To control the acceleration of the airflow at start-up of the flow in the main circuit by controlling the time for opening valve 3VE.

The air is carried in BISE by suction, using a vacuum pump with a nonadjustable flow rate (Rietschle SMV 500). The characteristics of the flow and pressure drop across the pump are determined both by the conditions of the flow test and by the pressure drop across the sampling filter and the rest of the circuit. Positioning the pump at the outlet of the circuit allows any additional turbulence in the flow to be avoided; it also allows the facility to be operated at a slight under pressure. We have tested the leak tightness of the apparatus in order to be sure that no external contamination, which could modify the observed phenomenon, is able to penetrate into the test bench.

The BISE test bench is electrically connected to earth in order to remove any possible charges attached to its walls. Finally, it is equipped with devices to measure and control the various environmental parameters inside the facility, humidity (RH), temperature (Temp) and pressure (Pr_1 and Pr_2). All of the data acquisition is carried out using a standard industrial computer. A special data acquisition program has been developed at the laboratory using LABVIEW software.

All of the measurements instruments used in BISE are listed in table 1.

Table 1 – Measurement instruments used in BISE

Measurement	Instrumentation or technique	Operating range	Precision of the equipment
Mean velocity (m/s)	High-frequency hot wire anemometry with probe 55P13 (Dantec)	2 cm/s – 500 m/s	± 0.1 % of measurement
Volumetric flow rate Q_v (m^3/h)	Turbine flow meter Fluxi 2100 (Schlumberger)	20-400 m^3/h	± 2 % of flow rate measurement for $20 < Q_v < 80$ m^3/h ± 1 % of flow rate measurement for $80 < Q_v < 400$ m^3/h
Air temperature (°C) Relative humidity (%)	Rotronic Hygrometer FT Series	0-50 °C 0-100 %	± 0.3 °C ± 1 % RH
Relative pressure (bar)	Intelligent pressure transmitter PR-53/80251 (Keller)	-1 to 0 bar	± 0.15 % of measurement range
Resuspended mass (g)	Balance MC210 P (Sartorius)	0-210 g	± 20 µg for 0 < m < 50 g ± 40 µg for 50 < m < 100 g ± 50 µg for 100 < m < 210 g

2.2. Aeraulic performance

Before undertaking experiments to investigate the fundamental parameters for resuspension of a particulate contamination, it is important to understand the aeraulic performance of the BISE facility in order to characterize the test air duct. This study consists of:

- evaluating the stability of the flow in the test duct,
- characterizing the velocity fields and the turbulence,
- describing the boundary layer in the test duct close to the powder deposit area:
- without obstacles,
- in the presence of an obstacle simulating a conical deposit,
- determining the characteristic shear velocities of the facility on the lower surface,
- determining the range of variation in acceleration at start-up of the airflow controlled by the electro-pneumatic valve, 3VE.

2.2.1. Measurement technique: Hot wire anemometry

In order to have an accurate local measurement of the velocity in BISE, we choose an intrusive measurement technique, a high-frequency hot-wire anemometer from Dantec. This measurement equipment includes a high-frequency anemometry unit (Streamline) and a calibration blower for the probes, all of which is controlled by a computer employing the associated StreamWare software. The system is illustrated in figure 3.

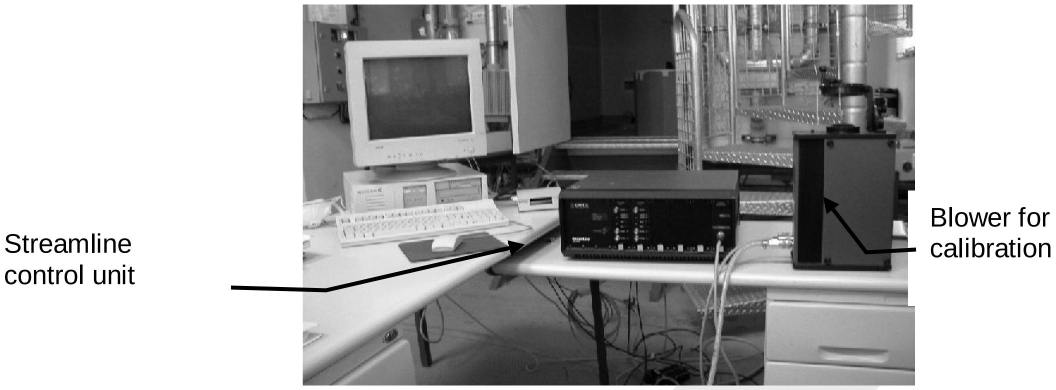

Figure 3 – The high frequency hot wire anemometry system (Dantec)

1.1.1.1 Measurement principle

The principle of hot wire anemometry is based on heat exchange between a hot metal wire and the airflow. It employs the relationship between electrical resistance and temperature.

When a tungsten wire, which has been heated to a certain temperature, is plunged into a fluid flow at a lower temperature, heat is exchanged between the wire and the air by convection. This exchange is a function of the velocity of the fluid and the temperature difference between the heated element and the fluid. It will modify the temperature of the wire and hence its electrical resistance and the voltage drop across it, in proportion to the velocity of the flow.

Because of its large velocity range (0.02 m/s to 500 m/s) and frequency (up to 400 kHz), the hot wire anemometer is able to measure the local instantaneous velocity and its fluctuations (and thus the turbulence intensity). This method is, therefore, well suited to our study which deals with the case of turbulent flows. Moreover, it has the advantage of not requiring the test bench to be seeded, in contrast to the optical methods initially considered.

However, location of the probes is particularly sensitive: the 5 µm diameter tungsten wires, 1.25 mm long, are very fragile and must be located very accurately with respect to the direction of flow.

1.1.1.2 The probe selected and its positioning in BISE

We arbitrarily define an orthogonal frame of reference (x, y, z) inside BISE, as follows:

- Ox: Axis parallel to the surface and normal to the flow,
- Oy: Axis parallel to the surface in the direction of flow (i.e. y corresponds to the principle component of the flow),
- Oz: Vertical axis normal to the surface.

The origin, O, of the reference frame is located on the lower surface at the centre of the test section (figure 2).

For our study, we use a wire probe or single wire (Dantec 55P13). This right angle probe is installed on a probe carrier, 55H21, which runs across the upper surface of the test duct in the test section. It takes measurements in the perpendicular plane at the hot wire position. Hence, in the BISE facility, it measures the principle component, v, along the y-axis, of the mean velocity of the free stream, V, the second component u (along the x-axis) being considered negligible (figure 4).

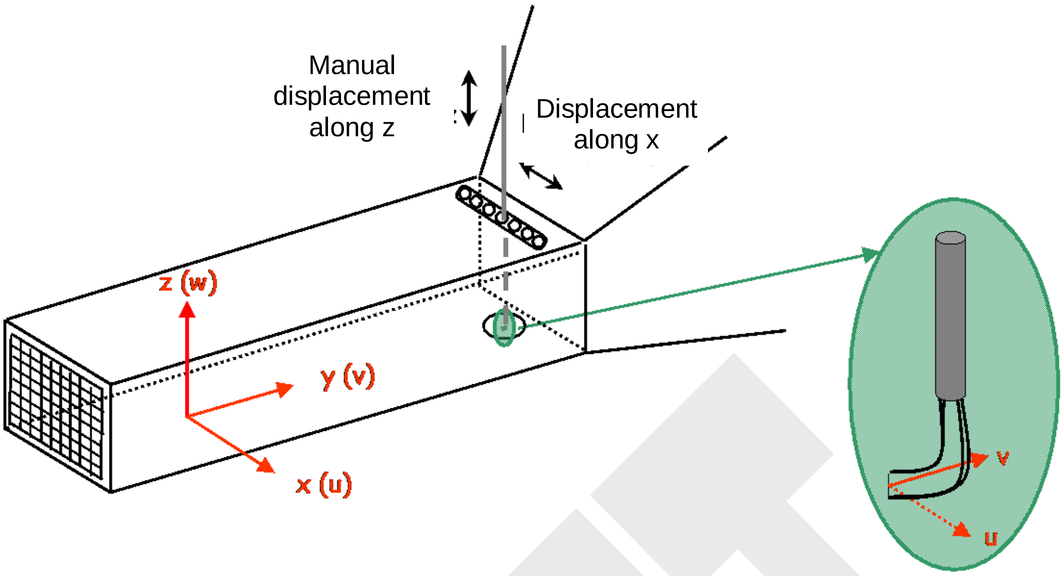

Figure 4 – Illustration of BISE with the hot wire anemometry instrumentation

The reference velocity, V, in our facility is measured at the origin of the frame of reference, at the exit and centre of the parallelepiped test duct, i.e. at (0; 0; 3.5 cm). This is virtually identical to the mean velocity V_∞ at the centre of the test section. A temperature compensation probe (reference 9090P01), is placed upstream of the parallelepiped test duct, in the airflow, in order to minimize the effects of drifts in the ambient temperature.

Calibration of the anemometry system is an essential phase for obtaining accurate measurements. This calibration is carried out regularly in the laboratory using the Dantec calibration blower. During the calibration process, it is important to align the probe to be calibrated with respect to the flow from the blower in the same way as it is aligned to the flow in the test air duct to be characterized.

1.1.1.3 Acquisition frequency

In order to measure the turbulence correctly, it is important to set an acquisition frequency for the measurements, which is higher than the timescale for the appearance of "bursts". Remember that these turbulent structures, similar to mini-tornadoes, can play a role in the phenomenon of lifting deposited particles. Blackwelder and Haritonidis (1983) describe the frequency of appearance of "bursts", f_b, using the relation:

$$f_b = 0.0035 \cdot \frac{v_*^2}{\nu} \qquad (1)$$

with v_*: shear velocity at the wall; ν: kinematic viscosity of the air.

Equation 1 requires us to know the shear velocity at wall. In BISE the hydraulic radius of the parallelepiped test duct, R_H, has a value of $4.421.10^{-2}$ m, and the maximum mean velocity, V_{max}, that can be attained is 15 m/s (the maximum velocity in the facility without a filter). From equation 16 (see § 2.2.4.1), the maximum Reynolds number for the flow attained in BISE has a value of around 87,500. It is, therefore, possible that the velocity distribution in BISE corresponds to a 1/7 power law inside the turbulent boundary layer (see equation 18). According to Schlichting (1979), the shear velocity at the wall, v_*, can then be calculated from the shearing rate, τ_0, for a turbulent flow travelling along a duct, according to the relation:

$$\tau_o = \rho v_*^2 = 0.0225 \rho V_\infty^{7/4} \left(\frac{\nu}{R_H} \right)^{1/4} \qquad (2)$$

with ρ: density of the air; V_∞: mean velocity of the free stream; R_H: hydraulic radius.

Under STP conditions ($\rho = 1.293$ kg/m^3 and $\nu = 1.515\times10^{-5}$ m^2/s), the shear velocity of the air at the wall becomes:

$$v_* = 0.06 \cdot V_\infty^{7/8} \quad . \qquad (3)$$

Then the frequence of appearance of "bursts" has the value for BISE of:

$f_b \sim 100$ Hz .

In order to operate at an acquisition frequency greater than the frequency for appearance of "bursts", our measurements are carried out at a frequency corresponding to 5 x f_b, i.e. 500 Hz.

According to the Dantec protocol, 2000 measurement points are sufficient to obtain the value of the mean velocity. However, for safety, we choose an acquisition procedure of 4000 points and perform five of these acquisition procedures at 500 Hz, spaced 4 seconds apart. These 5 acquisition procedures are repeated 3 times. The results presented below correspond to the mean of the measurements performed.

2.2.2. Stability and reproducibility of the flow

A first series of experiments consisted of evaluating the reproducibility of the flows obtained between two stops of the pump, the measurement being carried out with the volumetric flow meter. This information is important since it concerns the reproducibility of our resuspension results.

The measured coefficient of variation (ratio of the standard deviation over the mean flow rates) is of order of 2 % for flow rates greater than 140 m^3/h, i.e. a mean velocity V = 5 m/s in BISE. By contrast, it reached 8 % for flow rates around 10 m^3/h, i.e. V = 0.5 m/s in the facility. This is explained by the fact that this flow rate is below the calibration range of the flowmeter (see table 2).

A small drop in flow rate, of order of 5 %, is also noticed at the start of suction by the vacuum pump for a flow rate of 300 m^3/h. This is due to the stabilization of the vacuum pump. A delay of 15 minutes is proved to be necessary after starting the pump, in order to obtain good stability of the airflow (< 2 %) during experiments.

2.2.3. Turbulence velocity fields

Velocity measurements carried out at the limiting positions of valves PD_1 and GD_1 show that the velocities in BISE vary from 0.1 m/s to around 15 m/s, without the sampling filter. During our experiments, introduction of a sampling filter in the facility will create an additional pressure drop and hence modify the range of velocity variations in the facility. The range of BISE velocities in our experiments, therefore, depends on the pressure drop imposed by the type of sampling filter installed in the facility. A previous study (Witschger and Alloul-Marmor, 2001) showed that fibrous filters D-350 (Bernard Dumas) appeared best suited to our experimental study. These rectangular filters, with dimensions 204×253 mm^2, allow a mean velocity (investigated for our study) of 10 m/s in the facility. Moreover, they are not expensive. Other filters, reference 95-A from Bernard Dumas, are also used with the unique aim of carrying out experiments at higher velocities than 10 m/s (of order 14 m/s).

Further, measurements of the turbulence velocity fields in the test air duct were necessary in order to assure ourselves that the pile of powder present on the surface is uniformly exposed to the flow.

Investigation of these fields was carried out in the (y, z) plane at x = 0, by manual displacement of the anemometer probe. Along the Ox axis, seven cable glands able to hold the probe support, are spaced at locations 1.4 cm apart on the upper surface of BISE i.e. at x = -4.2 cm; -2.8 cm; -1.4 cm; 0 cm; 1.4 cm; 2.8 cm and 4.2 cm (Figure 4). Along Oy, movements are made manually using a calliper ruler to achieve a precision of 0.1 mm. To this uncertainty, must be added the error due to the manual nature of the action which is estimated at 0.5 mm. The maximum error in the position of the probe is therefore 0.6 mm.

Figure 5 shows the velocity fields and turbulence fields in the test air duct which we measured over cross-section (x, z) of the facility at y = 0. These measures were carried out for 3 air velocities measured at the centre of the duct of 0.5 m/s, 5 m/s and 10 m/s. For each of the fields, we have measured 42 points (7 positions across the width at 6 heights, z = 1 cm; 2 cm; 3 cm; 3.5 cm; 4 cm and 5 cm). The different colours in the velocity fields represent the difference in % between the value of the velocity at the considered point and the mean velocity at the centre of the cross-section, which we took as the reference value. The turbulence fields, on the other hand, are represented by their intensities. We recall that turbulence intensity is defined as the ratio of the instantaneous velocity fluctuations over the mean velocity. It is calculated as a coefficient of variation, i.e. as the per cent ratio of the estimation of the standard deviation of the instantaneous velocity, σ, over the mean velocity at the centre of the test section, V, i.e.:

$$I = \frac{\sigma}{V} \cdot 100 \quad . \qquad (4)$$

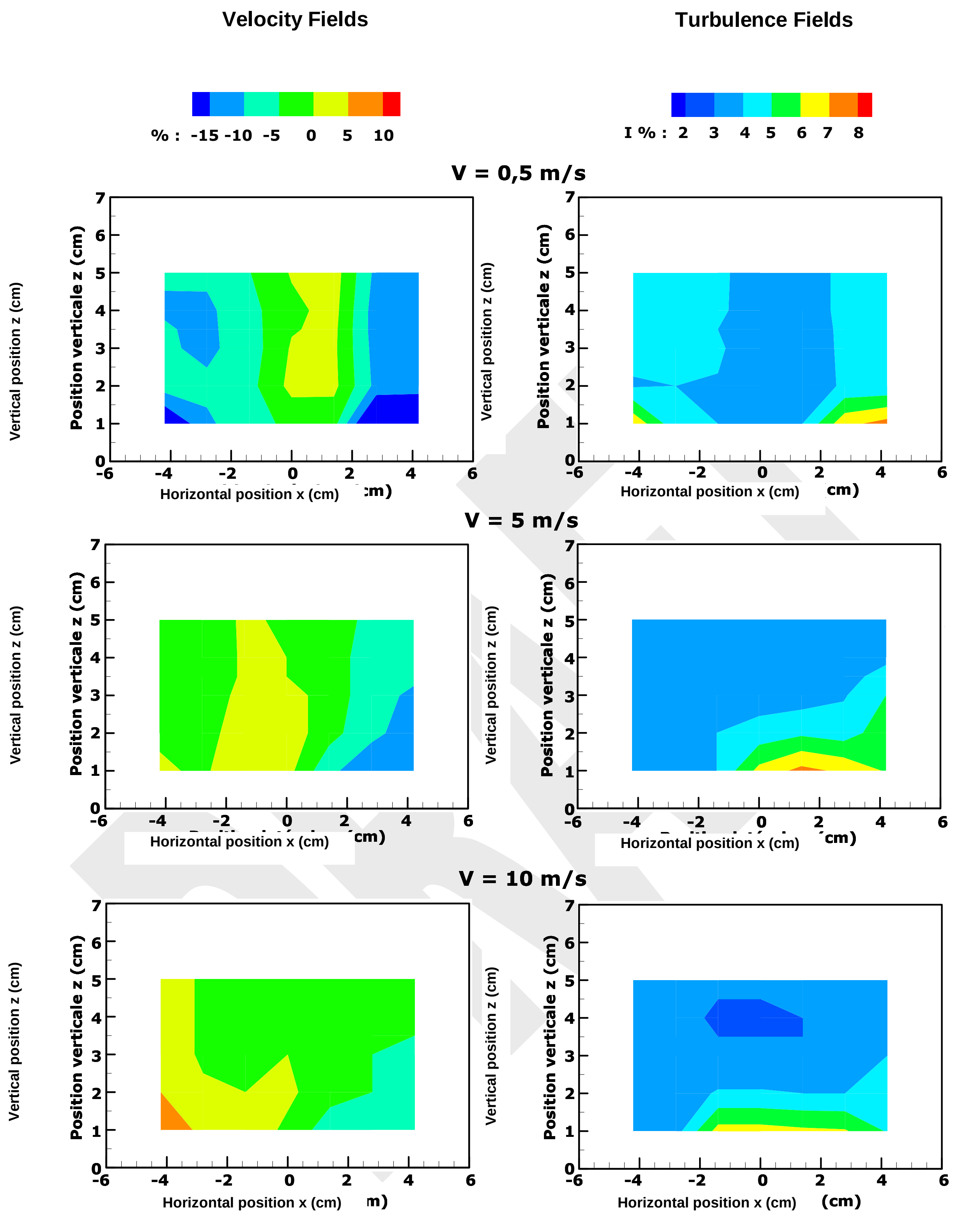

Figure 5 – Velocity fields (left) and turbulence fields (right) in the (x, z) plane at y = 0 expressed, respectively, as the difference with respect to the mean velocity, V, and as the intensity for three velocities V = 0.5, 5 and 10 m/s

These different graphs allow us to verify that the velocity profiles are relatively flat in the x direction. For the three velocities at the centre of the section, it can be seen that the values of the velocity differences remain in the interval ± 10 %. Our results also show that this spatial uniformity changes slightly with the velocity over all of the variation range.

For the turbulence fields, we note that whatever mean velocity is imposed in the facility, the turbulence intensity varies between 2 % and 5 % at the centre of the section. This indicates that the flow is stable at the centre of the test section.

However, the largest differences in the velocity are observed as the wall is approached. They reach approximately 10 % at 10 m/s and 15 % at 0.5 m/s. We also observe a slight increase in the turbulence intensity at z = 1 (I ~ 8 %). These gradients in the velocity and turbulence correspond to the classic profile for change in velocity close to a wall. They are due to the phenomenon of adherence of the fluid at the wall in the boundary layer (viscosity): velocities drop as the wall is approached and the turbulence intensity increases.

These results are important since, as we have seen and just like the turbulence in the vicinity of a pile of powder, the flow velocity has an influence on the phenomenon of resuspension by the airflow. The results indicate that the flow is homogeneous, uniform and stable at the centre of the duct. Moreover, the velocity profiles in this zone change only slightly over the entire range of variation of the airflow in BISE.

On the other hand, these results demonstrate the need to concentrate in a detailed way on what is occurring near the surface, at the point where the pile of powder will be deposited. Indeed, the modification to the profiles of the velocity and the turbulence, observed in the boundary layer, could have non-negligible effects on the process of powder resuspension.

2.2.4. Description of the boundary layer

To properly characterize the resuspension of particles, we need to fully understand the flow profile in the vicinity of the wall.

1.1.1.4 The boundary layer

In the case of flow of a viscous fluid (in our case, air) in the vicinity of a wall, the phenomenon of fluid adherence induces a strong velocity gradient at the wall. This area, in which the effects of the internal friction of the fluid are important, is the boundary layer. Outside of this layer, the fluid is said to be free.

The main flow that concerns us in problems of particle resuspension or wind erosion is turbulent flow which develops along the surface. We will, therefore, mostly consider the case of a turbulent boundary layer which develops on a flat plate. Schlichting (1979) and Rhyming (1991) among others, present similar models for the development of this type of flow, which are now relatively well-known.

When the boundary layer starts at y = 0, the flow inside the boundary layer initially develops in a laminar fashion. Then, after a transition region, it becomes more unstable, transforming into the turbulent region. The transition is accompanied by a sharp increase in the thickness of the boundary layer and it depends, in the case of a flat plate, on the value of the local Reynolds number, Re_y:

$$Re_y = \frac{V_\infty \cdot y}{\nu} \quad , \tag{5}$$

where y is the distance after which the boundary layer is formed and V_∞ the characteristic mean velocity of the flow outside the boundary layer. The transition occurs for a local Reynolds number of order of 10^5 to 10^6 (Ryhming, 1991).

When boundary layer turbulence is established, it consists of an internal layer close to the wall representing 5 % to 15 % of the thickness and an external region formed by the remaining 85 % - 95 %. In the case of resuspension, it is essentially the internal region which will play a role in the detachment of particles. Indeed, it is in this region close to the wall, that the flow will interfere with the bed of particles.

Within the internal region, it has been shown experimentally that the distribution of velocities in the layer consists of three distinct regions:

- the laminar sublayer, which is the region closest to the wall. It is uniquely characterized by the effect of laminar shear constraints. Because, however, of the unstable nature of the flow in this zone, the term viscous sublayer is more appropriate.
- the transition region, the connecting region between the viscous sublayer and the logarithmic region,
- the logarithmic region which is the region where the flow is entirely turbulent.

The profile inside each region is described by:

$$v+ = f(z+) \quad . \qquad (6)$$

Hence, in the internal zone we have:

- the viscous sub-layer: $v+ = z+$ for $0 < z+ < 5$, (7)
- the transition region: $v+ = 5\ln(z+) - 3{,}05$ for $5 < z+ < 30$, (8)
- the logarithmic region: $v+ = 2{,}5\ln(z+) + 5{,}5$ for $30 < z+ < 500$, (9)

where $v+$ is a dimensionless velocity corresponding to the axial component of the velocity according to equation 10:

$$v+ = \frac{V_\infty}{v_*} \quad . \qquad (10)$$

The variable z+ is defined according to $z+ = \frac{v_* \cdot z}{\nu}$. It corresponds to the vertical position starting from the surface.

Beyond z+ = 500, is the external region or low velocity region, strongly linked to the conditions outside the boundary layer. The characteristic values in this region are the height of the boundary layer, δ, and the velocity outside the layer.

It follows that the general distribution of the velocities for a turbulent boundary layer may be represented by a single curve of $v+ = f(z+)$ linking the different regions of the boundary layer (figure 6). It is customary to represent this set of curves in semi-logarithmic coordinates, in order to clearly distinguish the different regions. All these laws are valid for flows over a smooth wall.

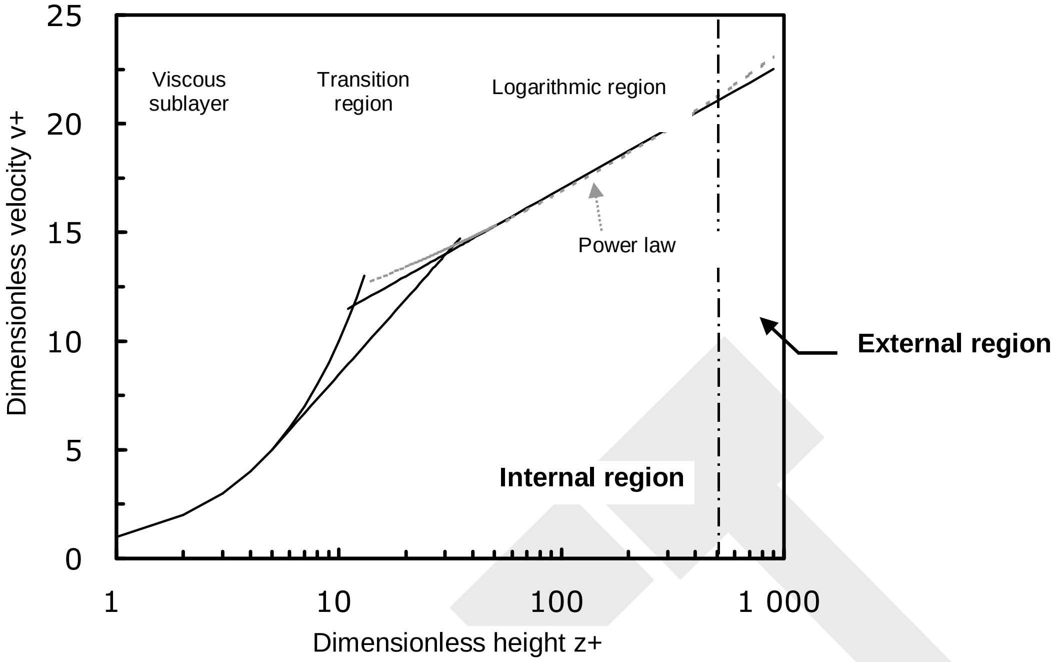

Figure 6 – Calculations of the distribution of v+ as a function of z+, in the internal region of a turbulent boundary layer

The universal distribution thus described is rather complex but it has the advantage of also applying to a flow under development. However, for certain practical cases, it is sufficient to use a more approximate velocity profile in the form of a power law:

$$\frac{v}{V_\infty} = \left(\frac{z}{\delta}\right)^{1/n} , \qquad (11)$$

where δ: thickness of the boundary layer; n: exponent, function of the value of the Reynolds number.

In the case of a flat plate, n ~ 7 (Schlichting, 1979). This power law has been suggested by the following experimental result:

$$v+ = 8.74(z+)^{1/n} . \qquad (12)$$

This power law distribution, observed in figure 6, clearly represents the logarithmic region of the universal law. However, it is unable to describe in as much detail as the universal law, the velocity profile within the viscous sublayer in the immediate vicinity of the wall.

Friction at the wall plays an important role in the process leading to the universal distribution of velocities. Experimentally determined from the gradient of the logarithmic law, reformulated as a function of V_∞ , the coefficient of friction, C_f, is a function, in particular, of the roughness of the surface and of the established character of the flow. By using the expression for the shear velocity, in the case of a flat plate, we obtain:

$$C_f = 2\frac{\tau_0}{\rho {V_\infty}^2} = 0.045\left(\frac{V_\infty \delta}{\nu}\right)^{-1/4} . \qquad (13)$$

Another characteristic to consider is the thickness of the boundary layer, δ. This is generally defined by the distance to the wall where the velocity is equal to 99 % of the value of V_∞. It depends on several factors such as the viscosity of the fluid and the degree of turbulence.

In the case of a laminar boundary layer, the velocity distribution is parabolic. For a flat plate, its thickness is given by the Blasius solution (Ryhming, 1991):

$$\frac{\delta}{y} = 4.96\,\mathrm{Re}_y^{-1/2} \quad . \tag{14}$$

In the case of a turbulent boundary layer, the velocity distribution is considerably more flattened. For a perfectly flat surface, the thickness of the turbulent boundary layer is therefore determined by the empirical formula:

$$\frac{\delta}{y} = 0.37\,\mathrm{Re}_y^{-1/5} \quad , \qquad \text{with } 10^5 < \mathrm{Re}_y < 10^7 \quad . \tag{15}$$

If the case of the parallelepiped duct is considered, the flow regime is determined by the Reynolds number relative to the hydraulic diameter, D_H, of the duct and the velocity at the centre of the flow, V, according to the equation:

$$\mathrm{Re} = \frac{V D_H}{\nu} \quad , \tag{16}$$

with

$$D_H = \frac{4S}{L} \quad , \tag{17}$$

where S: cross-section of the duct; L: perimeter of the section.

When the Reynolds number is higher than 2100, the flow which was until then laminar tends to become turbulent (Midoux, 1985). However, a transition region is observed at Reynolds numbers between around 1500 and 3000.

In turbulent conditions, a power law describes the velocity profiles well. It is written in the form:

$$\frac{v}{V} = \left(\frac{z}{R_H}\right)^{1/n} \quad . \tag{18}$$

The values of n are, therefore, a function of the Reynolds number for the duct. Let us indicate some values of n:

n	**Re**
6	4×10^3
7	1.1×10^5
10	2×10^6

However, in the vicinity of the entry to the parallelepiped duct, the velocity, V, is dependent on the axial component, y, and does not describe the velocity profiles of a turbulent flow. It is necessary to consider an establishment length, which corresponds to the development of the boundary layer inside the duct. If this length is reached, the regime is said to be *established*, i.e. the velocity profile no longer depends on the distance from the entrance of the duct. In contrast to the laminar regime, the flow velocity in the turbulent regime is such that the boundary layer cannot cover the entire cross-section of the duct. First, there is the development of the turbulent boundary layer at a point T, then the turbulent regime is established when its thickness reaches a value close to $0.2D_H$. The establishment length Le or the length to develop the velocity profile in turbulent flow, thus has the value:

$$L_e = 0.46 D_H Re^{1/4} \quad . \tag{19}$$

The central region exhibits an almost flat profile. An illustration of the development of the turbulent boundary layer is shown in figure 7.

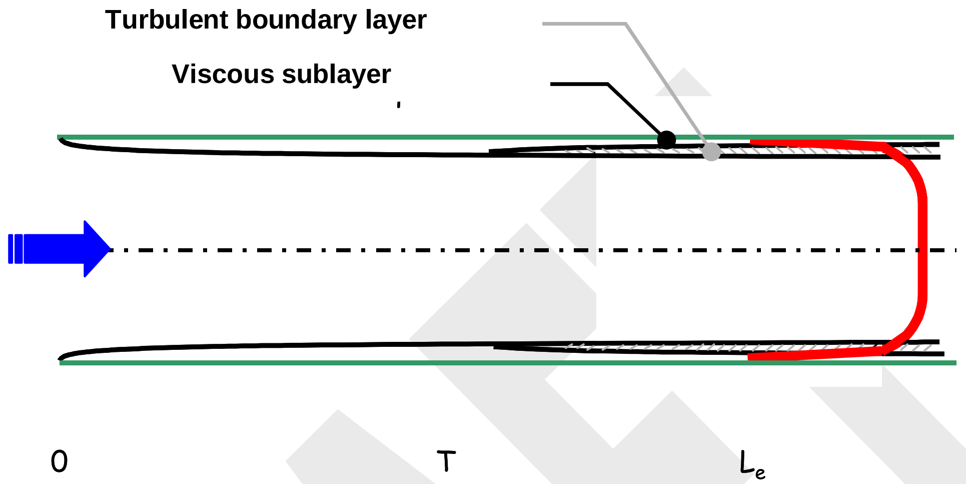

Figure 7 – Establishment of the velocity profile in a duct under turbulent flow

In our situation, where we are interested in resuspension of particles deposited in a pile on the surface, it can be assumed that the boundary layer which will develop on the surface will have its characteristics modified. Indeed, the pile of powder may be comparable with a natural roughness of the surface, likely to modify the velocity profiles, in particular in the internal zone (Foucault, 1994). We recall that the reference for material roughness, used by Nikuradse, for established flows in pipes, is the grain of sand (Midoux, 1985; Ryhming, 1991).

However, from an aeraulic point of view, we will treat the presence of the powder pile in BISE as an obstacle introduced into the facility. We will limit ourselves to a detailed description of the boundary layer in the test duct without obstacles, in order to determine the singularities of the facility, to find out whether the flow regime is established or not, to determine the various boundary layer thicknesses and, above all, to calculate the shear velocities from the velocities measured in the boundary layer. Hence, we will mainly characterize the flow incident on the powder pile. However, measurements are also carried out in the presence of an obstacle in order to observe the development of velocity profiles under these conditions.

1.1.1.5 Experimental measurements

We carry out the velocity measurements close to the surface in the central zone of the test section, at the powder bed location, i.e. for x = 0 and y = 0. Figure 8 depicts the normalized vertical profiles of the velocities in BISE, for the three velocity values at the centre of the cross-section V = 0.5 m/s, 5 m/s and 10 m/s. The anemometer probe selected, allows us to approach within 1 mm of the wall along the Oz axis, in order to describe the boundary layer. H corresponds to the height of the parallelepiped duct, i.e. 7 cm.

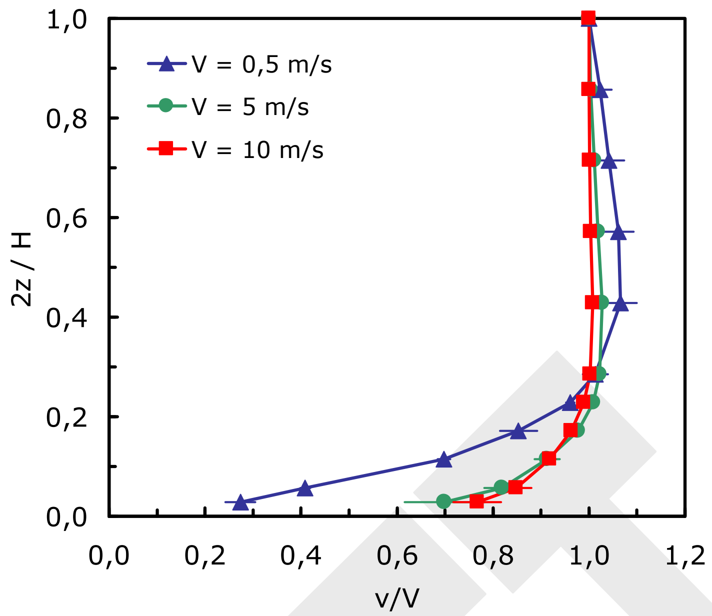

Figure 8 – Velocity profiles close to the surface at x = 0 for V = 0.5 m/s, 5 m/s and 10 m/s

For velocities of 5 m/s and 10 m/s, the normalized velocity profiles observed are relatively flat; the flow seems to clearly follow a turbulent regime profile. By contrast, at 0.5 m/s, we notice that the velocity profile is much more rounded. It can, therefore, be supposed in this case that the profile is much closer to the laminar regime.

From the three velocities, it is possible for us to determine certain characteristics of the flow. In particular, we can calculate the Reynolds number of the flow, Re, in the test duct and the establishment length Le of the velocity profile, defined by equations 16 and 19 respectively. These data are listed in Table 2.

Table 2 – Characteristics of the airflow in BISE for three velocities 0.5, 5 and 10 m/s

V (m/s)	Re (-)	L_e (cm)
0.5	2900	-
5	29200	54
10	58400	64

This table confirms our initial assumptions. Indeed, we note that, for 5 m/s and 10 m/s, the Reynolds numbers for the duct are much higher than 3000 (~30,000 and ~58,000). The flow is therefore clearly turbulent in this velocity range. However, in these configurations, the lengths required to establish the turbulent regime in the test air duct have values of 54 cm and 64 cm, respectively. On the other hand, the BISE facility has a length of only 38 cm up to the centre of the test surface to allow a boundary layer to develop. As a consequence, the turbulent regime is not totally established in BISE; this explains why the velocity profiles in figure 8 are not entirely flat. Apart from the fact that these profiles are dependent on the distance to the entrance of the duct, this will not have any influence on the experimental results.

For the velocity profile at 0.5 m/s, the associated Reynolds number in the duct has a value of 2900. Hence, the flow is in the transition region between the laminar and turbulent regimes. The velocity profile observed in figure 8, nevertheless suggests that the regime is already very laminar. In this case, the establishment length for the parabolic profile has a value of around 10 m. There too, the regime is not established.

We also measure the vertical profiles of the turbulence intensity (see equation 4) close to the wall for velocities of 0.5 m/s, 5 m/s and 10 m/s at the centre of the section. These are presented in figure 9.

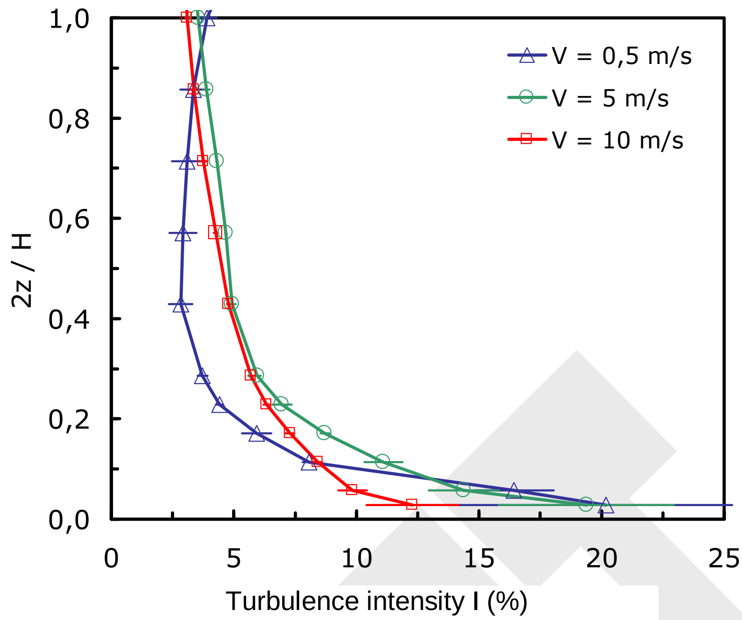

Figure 9 – Turbulence intensity profiles close to the surface for x = 0 at V = 0.5 m/s, 5 m/s and 10 m/s

The profiles show that the turbulence intensity reaches 10 % to 25 % as the lower surface is approached, whatever the mean velocity set in the facility; the flow is therefore unstable and irregular at the boundary layer. For heights greater than 1 cm (i.e. $\frac{2z}{H} \geq 0.3$), values can be found for turbulence intensity (from 2 % to 5 %), as seen in the plots of figure 5.

In order to characterize the internal region of the boundary layer, we also plot in a semi-logarithmic representation, the normalized velocity profiles measured with the hot wire anemometer (figure 10), as a function of the three mean velocities at the centre of the facility 0.5 m/s, 5 m/s and 10 m/s. Each profile has been measured twice.

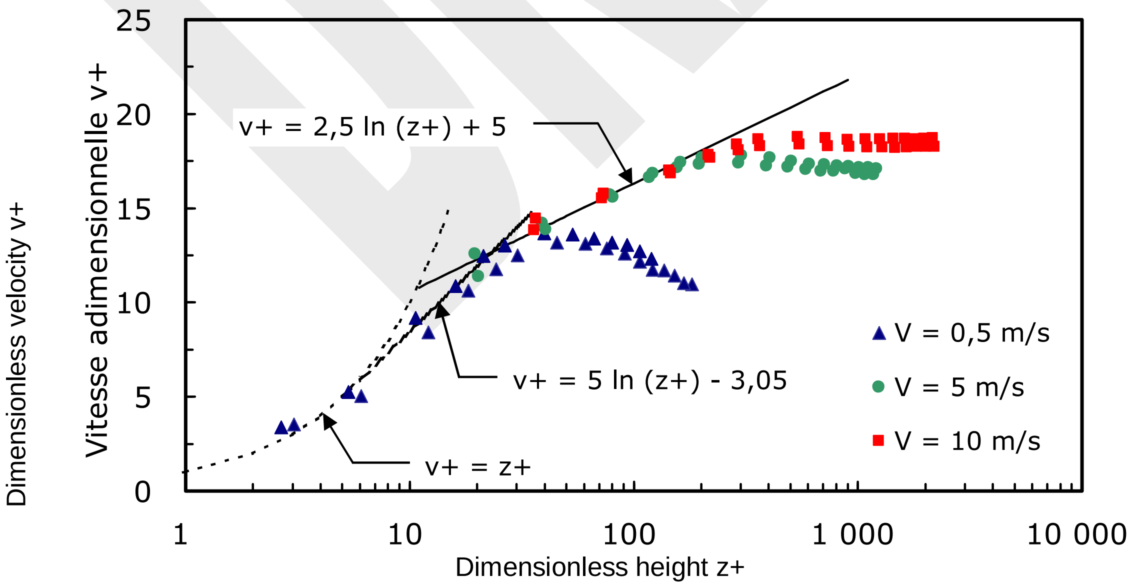

Figure 10 – Normalized volocity profiles in semi-logarithmic representation at x = 0 and y = 0 for various mean velocities

We can see that the measured velocities are in good agreement with the results from the literature for a turbulent boundary layer at a flat plate.

There are three distinguished zones in the internal region:

- the viscous sublayer where $v+ = z+$ for $0 < z+ < 5$,
- the transition region where $v+ = 5\ln(z+) - 3.05$ for $5 < z+ < 30$,
- the logarithmic region where $v+ = 2.5\ln(z+) + 5$ for $z+ > 30$. (20)

However, in the logarithmic region, equation 20 determined in BISE, fits our results better than equation 9, valid for a perfectly flat surface. This relation differs in its second term (5 in place of 5.5). This small difference can be attributed to a protrusion (roughness) coming either from the edge of the test surface or the space (even though it is very small) between the test surface and the base of the facility.

Finally, we note that for z+ > 200, the measurements we carried out at velocities of 5 m/s and 10 m/s in strongly turbulent flow, do not follow the logarithmic law. This can be explained by the fact that only the velocity profile close to the wall can be approximated to the flat plate case.

Since we are able to compare the velocity profiles close to the surface in the case of a flat plate, we can determine the thickness of the boundary layer from expressions 14 and 15. These thicknesses, calculated for the specific establishment length of BISE, 38 cm, are reported in table 3.

Table 3 – Values for the thickness of the boundary layer at various velocities

V (m/s)	Re_y (-)	δ (mm)
0.5	14000	17
5	133400	13
10	255400	12

These values of the thickness of the boundary layer are important in the phenomenon of resuspension since, in particular, they determine the flow characteristics close to the powder deposit. This will not always be exposed to the same velocity profile, depending on whether or not its height is greater than the thickness of the boundary layer. It was, therefore, important to be able to correctly characterize these values.

1.1.1.6 Shear velocity

The description of the boundary layer also allows us to determine the characteristic shear velocities, v_*, in BISE. The results of measurements carried out close to the surface indicate that the profiles are relatively similar to those of a flat plate. From these results, we determine the characteristics shear velocities, v_*, in BISE using two different methods.

✓ *The gradient method at the origin:*

Using this method, shear velocities are obtained from the velocity gradient for a velocity measurement carried out close to the wall.

✓ *The Bradshaw method:*

This method, which is not used very often, is described by Leprince *et al.* (1985). It consists of finding the point on the experimental velocity profile which corresponds to a fixed value of the dimensionless height, z+, in the region of the boundary layer described by a logarithmic law. The shear velocity is then obtained graphically from the dimensionless velocity v+ at the same point.

Figure 11 shows the shear velocities, v_* obtained by the Bradshaw method and the gradient method at the origin, as a function of the reference velocity, V, at the centre of the test section. For each of the two methods, two series of measurements were carried out.

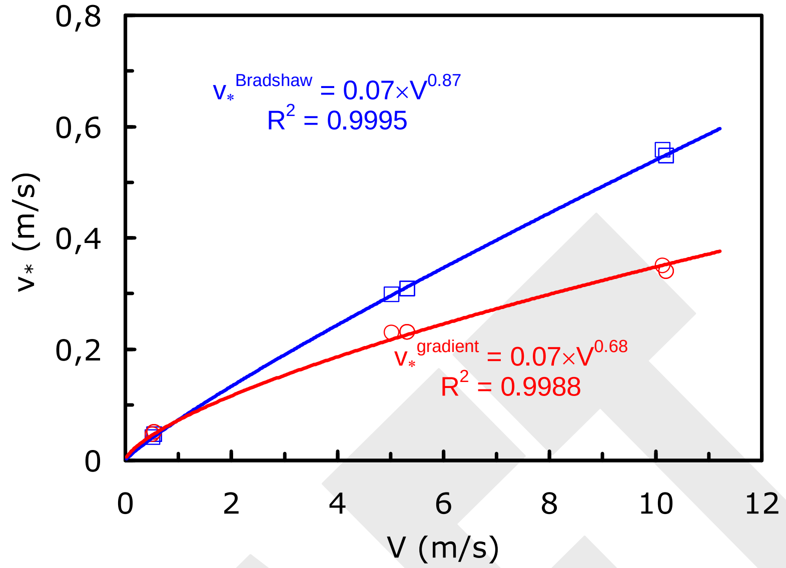

Figure 11 – Change of shear velocity at the wall, v_*, as a function of the mean velocity, V, in the BISE facility

We see that the gradient method gives a shear velocity less than that of Bradshaw, the difference increasing as a function of the mean velocity. Indeed, for 5 m/s < V < 10 m/s, the difference obtained between the two methods varies between 20 % and 35 %. We attributed the shift to the gradient method, which requires that the point used to calculate the shear velocity is in the laminar sublayer at z+ < 5, corresponding to z = 2.2 mm for 0.5 m/s and z = 0.3 mm for 10 m/s. However, as we have previously seen, our positioning system does not allow us to place the anemometer probe lower than z = 1 mm. The Bradshaw method, on the other hand, does not require a precise determination of the region of the logarithmic law. Comparative studies (Leprince *et al.*, 1985) show that the Bradshaw method gives more precise values for the shear velocity. Moreover, the measurements that we carried out in BISE, using an anemometer probe having a different geometry, confirm this tendency.

A fit of the experimental points allows us to deduce correlations between the shear velocity and the mean velocity in the test duct. The correlation that we will use for the BISE facility is, therefore, that obtained by the Bradshaw method on the two series of experiments carried out, namely,

$$v_* = 0.07 \times V^{0.87} \quad . \qquad (21)$$

For velocities varying from 0.5 m/s to 10 m/s, the shear velocity of the air at the wall, v_*, varied from 0.05 m/s to around 0.6 m/s.

A comparison can be made between this expression for the shear velocity (21) and the theoretical calculation of equation 3. Comparing the mean velocity of the facility with the velocity at the centre of the test duct, we notice that these two expressions are very similar. The similarity of these expressions confirms the choice that we have made to adopt the Bradshaw method (and not the gradient method) to determine the shear velocities in the facility.

1.1.1.7 The boundary layer in the vicinity of a conical obstacle

Of course, the introduction of a powder bed into the facility will modify the flow characteristics. In order to be able to observe the change in the velocity profile close to the deposit, we have made an aluminium mould of identical shape and dimensions to the powder pile that we use in our experiments. This is then placed in the facility on the test surface and measurements of velocity and turbulence are performed with a hot wire anemometer in the vicinity of the cone. Our results for a mean velocity of 10 m/s in the (y, z) plane at x = 0 are shown on the plots in figure 12. In section 2.2.3, we noted that the velocities were relatively homogeneous in this section. Hence, following several preliminary trials over the entire cross-section, we then carried out measurements restricted to the region –2 cm ≤ x ≤ 0 cm by displacing the cone, and not the probe, along x. This gave us a large number of measurement points in this direction. Indeed, the cable glands positioned in the facility (see figure 4) require measurements at separations of x = 1.4 cm. This method allows us to reduce this interval to x = 0.5 cm. Our experimental points are then shown by symmetry following a vertical axis centred on x = 0.

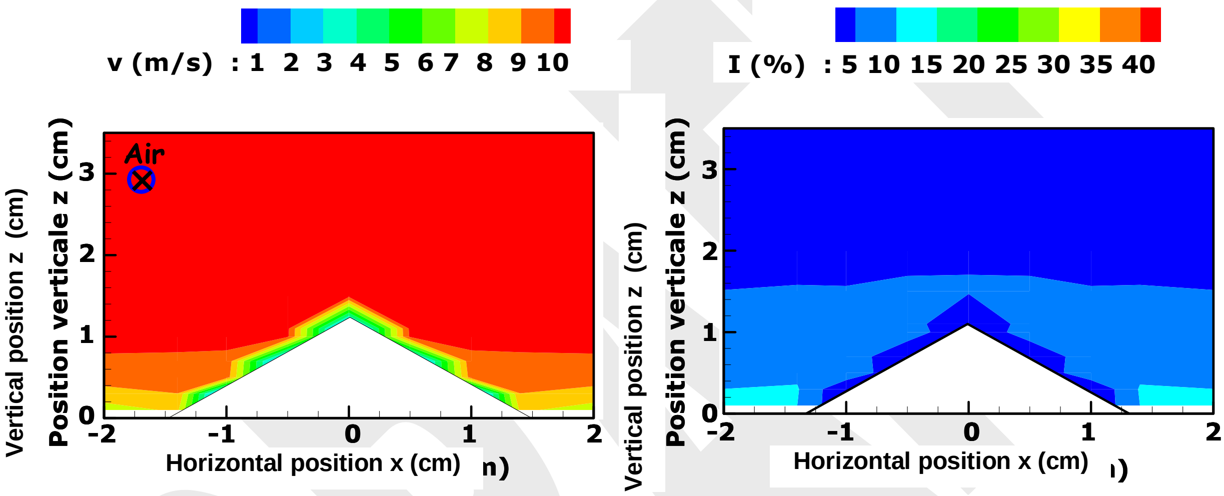

Figure 12 – Velocity fields (left) and turbulence fields (right) in cross-section (x, z) at y = 0, in the presence of and close to the surface of a conical obstacle, for a mean velocity of 10 m/s

The irregular curve observed on the graphs stems from an artefact linked to the representation. It is not possible to interpolate values between two actual measurements; hence the steps appear as a "staircase".

In the plane perpendicular to the airflow, the velocity field close to the wall and in the vicinity of the conical obstacle shows that a boundary layer develops along the surface of the cone. This boundary layer is parallel to the surface of the cone and, because of the gradient, the shear velocity, v_*, increases from the base to the summit of the pile. Meanwhile, the turbulence intensity is only slightly modified by the presence of the cone in cross-section (x, z); it is less than 5 % in the central part of the test duct and tends towards 15 % close to the surface of the facility.

We also carried out velocity and turbulence measurements for a mean velocity of 10 m/s with the simulation cone in the (y, z) plane, i.e. in the principle flow direction. To do this, we will consider that over several centimetres the velocity profile only changes very slightly. Hence, and as before, our measurements are carried out by displacing the cone along the y axis, its centre being at x = 0. The results are presented as velocity and turbulence intensity in figure 13.

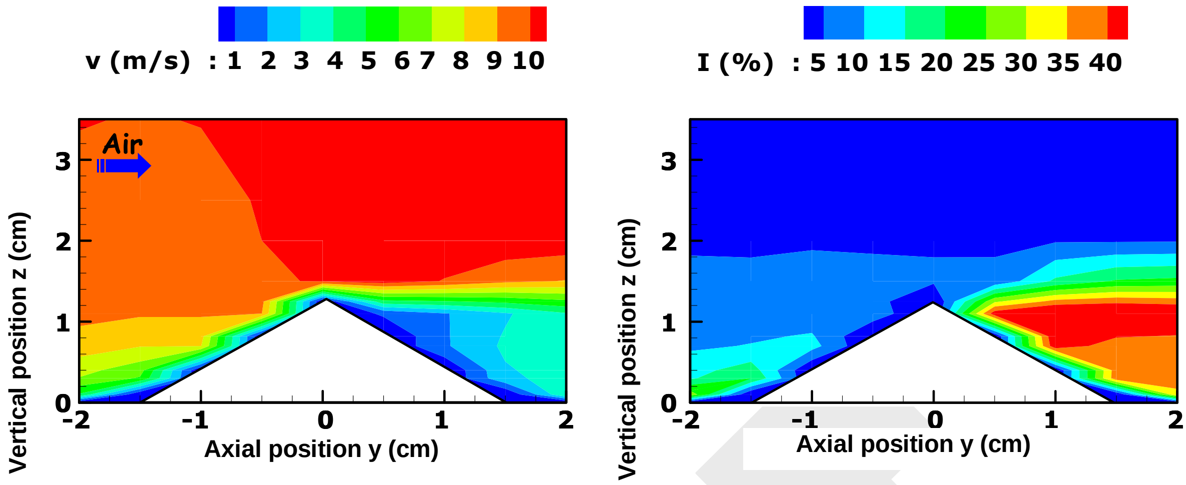

Figure 13 - Velocity fields (left) and turbulence fields (right) in cross-section (y, z) at x = 0 in the presence of and close to the surface of a conical obstacle for a mean velocity of 10 m/s

As expected, the presence of the cone in the cross-section (y, z) modifies the flow characteristics close to the surface, in a non-negligible way. Indeed, at the centre of the section, there is a relatively homogeneous velocity associated with very low turbulence intensity (< 5 %). By contrast, around the cone the flow properties differ.

We now need to separate this phenomenon, from an aeraulic point of view, into two parts:

- upstream of the pile, i.e. on the face of the cone directly facing into the air flow.
- downstream of the pile, i.e. on the face of the cone sheltered from the air flow.

Upstream, we observe, as in figure 12, that a boundary layer develops along the surface of the conical mould. However, this is thicker and a larger turbulence is associated with it, since it reaches 25 %.

Immediately downstream from the bed, we observe a shear zone which touches the summit of the cone, and a recirculation zone of the air. This recirculation zone is located behind the cone subjected to the flow and is shaped by a large eddy (or wake). In this depression zone sheltered from the wind, whose height is less than that of the cone, we observed a rapid drop in velocity (down to 1 m/s) and the rate of turbulence is very high.

2.2.5. Acceleration

Finally, the facility can control the acceleration during start-up of the airflow in the main circuit using an electro-pneumatic valve with adjustable opening speed. The rotation of the solenoid valve is achieved by a double acting (air to air) pneumatic actuator (Keystone type 79D-012).

Our velocity measurements of the rotation of the valve show that the acceleration is dependent on the velocity imposed in the main circuit. The accelerations α are determined from the establishment curves for the air velocity in the main circuit. These are measured by anemometry at an acquisition frequency of 500 Hz. For example, figure 14 shows changes with respect to time in the velocity during start-up of the airflow in BISE, for an imposed velocity of 7.5 m/s (i.e. $v_* = 0.4$ m/s). One is measured at minimum acceleration, i.e. $\alpha_{min} = 0.3$ m/s^2, while the other corresponds to maximum acceleration, i.e. $\alpha_{min} = 20$ m/s^2.

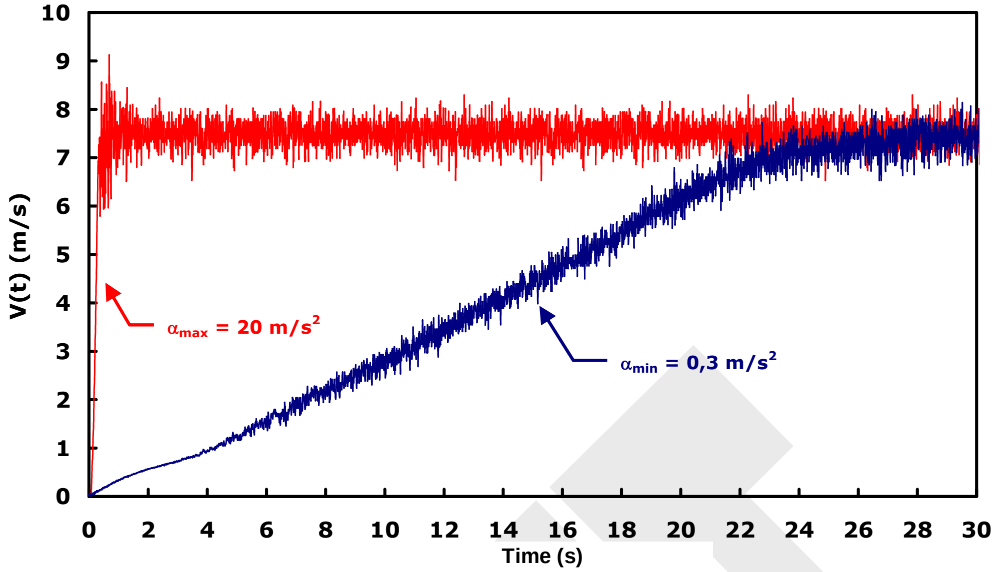

Figure 14 - Changes as a function of time in the velocity during start-up of the air flow in BISE for an imposed mean velocity of 7.5 m/s

We calculate the acceleration by analyzing the gradient of the increase in velocity. We note that for high acceleration, the transition phase very rapidly generates large fluctuations in the instantaneous velocities. Because of this, the instantaneous velocities can, over a very short period, be significantly higher than the target air velocity for the tests.

Table 4 gives the ranges of variation in acceleration for different air velocities.

Table 4 - Range of variation in acceleration during start-up of the airflow for various velocities

V (v_*) (m/s)	α_{min} (m/s^2)	α_{max} (m/s^2)	$\frac{\alpha_{max}}{\alpha_{min}}$
0.5 (0.04)	0.05	2.6	~50
5 (0.28)	0.3	14.2	~50
7.5 (0.40)	0.3	20.0	~70
10 (0.52)	0.5	31.0	~60

We know that, for a specific air velocity, the acceleration varies by a factor of around 50 to 70. On the other hand, the ranges of acceleration change with the stabilization velocity: for V = 0.5 m/s, the acceleration α varies from 0.05 m/s^2 to 2.6 m/s^2, whereas it is between 0.5 m/s^2 and 31 m/s^2 for a velocity of 10 m/s.

3. CONCLUSIONS

We have developed an experimental facility within which the air can be conveyed in a velocity range between 0.5 m/s and 15 m/s, and in which the acceleration of the airflow at start-up is controlled. This device is also equipped with various measurement sensors, enabling control of environmental parameters such as temperature, humidity and pressure.

Our aeraulic measures show that the BISE test bench possesses good temporal stability and good spatial uniformity at the centre of the test section, in the region where the powder bed will be deposited. The use of hot wire anemometry has allowed us to characterize the velocity and turbulence profiles close to the surface. Our results are in good agreement with the literature for a turbulent boundary layer at a flat plate. From these measurements, we have been able to determine the important characteristics of the facility and to determine the shear velocities and the thicknesses of the boundary layer in the test air duct. These essential characteristics of our study will therefore be used to determine the conditions for resuspension, by an airflow, of particles coming from a powder deposit.

Finally, our velocity and turbulence measurements carried out close to a conical obstacle, simulating a pile of powder, show how much the addition of an obstacle in the test duct contributes to modification to the velocity profile close to the surface. They also made it possible to see that resuspension, which is strongly dependent on this modified profile, is a phenomenon as complex as one could have feared.

REFERENCES

Alloul-Marmor, L. (2002), Réentrainement par écoulement d'air d'une contamination particulaire déposée sur une surface. Thèse de doctorat de l'Université Paris XII.

Biasi, L., De Los Reyes, A., Reeks, M. W., De Santi, G. F. (2001), Use a simple model for the interpretation of experimental data on particle resuspension in turbulent flows. *J. Aerosol Sci.*, **32**, 1175-1200.

Blackwelder, R. F., Haritonidis, J. F. (1983), Scaling of the bursting frequency in turbulent boundary layers. *J. Fluid Mech.*, **132**, 87-103.

Braaten, D. A. (1994), Wind Tunnel Experiments of Large Particle Rentrainment - Deposition and Development of Large Particle Scaling Parameters. *Aerosol Sci. Technol.*, **21**, 157-169.

Foucault, J. M. (1994), Etude théorique et expérimentale des phénomènes d'envol et de saltation de particules dans une couche limite turbulente. *Thèse de doctorat*. Université des Sciences et de Technologies de Lille, 6 octobre 1994.

Friess, H., Yadigaroglu, G. (1998), Inclusion of Structural Parameters in the Modelling of Aerosol Resuspension. *Third OECD Specialist Meeting on Nuclear Aerosols in Reactor Safety*. Cologne, Germany, 15-18 June, 1998.

Fromentin, A. (1989), Particle resuspension from a multi-layer deposit by turbulent flow. *Thèse de doctorat*. Paul Scherrer Institut. **PSI-Bericht Nr. 38**, September 1989.

Hall, D. (1989), The time dependence of particle resuspension. *J. Aerosol Sci.*, **20**, 907-910.

Leprince, F., Riethmuller, M. L. (1985), Skin determination by LDV measurements in a viscous sublayer – Analysis of systematic errors. *Technical note 156, Von Karman Institut for Fluid Dynamics*, December 1985.

Midoux, N. (1985), Mécanique et Rhéologie des fluides en génie chimique. *Technique et Documentation (Lavoisier), Paris*.

Reeks, M. W., Hall, D. (2001), Kinetic models for particle suspension in turbulent flows : theory and measurement. *J. Aerosol Sci.*, **32**, 1-31.

Ryhming, I. L. (1991), Dynamique des fluides. *Edité par Presses polytechniques et universitaires romandes, Seconde édition*.

Schlichting, H. (1979), Boundary-Layer Theory. *Septième édition, Mc Graw-Hill, New York.*

Witschger, O., Alloul-Marmor, L. (2001), Evaluation de la perte de charge de trois types de filtre B. Dumas. *Rapport technique DPEA/SERAC/LPMAC/01-14, IPSN*.

4. Annexes

Annex 1 – Document approval by beneficiaries' internal QA

4.1. Annex 1: Document approval by beneficiaries' internal QA

Fill involved beneficiaries as appropriate (mandatory for Milestones and Deliverables, but optional for other document type)

#	Name of beneficiary	Approved by	Function	Date
1	IRSN	Norbert Kohtz (TUV – Rheinland)	SP leader	12/03/12
2		Christoph Pohl (TUV Rheinland)	formal approval according to the ARCHER template	15/10/12
3				
4				
6				
7				
8				
9				
10				
11				
12				
13				
14				
15				
16				
17				
18				
19				
20				
21				
22				